Investigation of the electromechanical behaviors in Cu-stabilized GdBCO coated conductor tapes using high-cycle fatigue tests at 77 K and related fractographic observations

Hyung-Seop Shin ⓘ, Michael B de Leon and Mark Angelo E Diaz

Department of Mechanical Design Engineering, Andong National University, Andong, Kyungbuk, 36729, Republic of Korea

E-mail: hsshin@anu.ac.kr

CrossMark

Abstract

In applications employing high-temperature superconducting conductors, various cyclic loading (fatigue) conditions produced by mechanical, thermal, or periodic electromagnetic forces are inevitable. Applying coated conductor (CC) tapes under fatigue loading conditions is expected to critically affect the long-term reliability of its superconducting performance. Most studies evaluating the mechanical and electromechanical characteristics use quasi-static uniaxial tensile tests. Few have focused on the characterization of CC tapes under fatigue loading. In this study, the electromechanical property characterization of Cu-stabilized $GdBa_2Cu_3O_y$ (GdBCO) CC tapes including fatigue behaviors were investigated at 77 K. High-cycle uniaxial fatigue tests were carried out on GdBCO CC tapes 4 and 12 mm in width, and the two were compared in terms of mechanical and electromechanical aspects at a stress ratio of 0.1. The mechanical and electrical fatigue limits of the CC tapes were determined at 77 K. The 4 mm wide CC tapes showed less fatigue limits when compared to the 12 mm wide ones. However, regardless of the CC tape width, the sequence in the obtained characteristic strengths at 77 K was the same: yield strength $>$ irreversible stress limit $>$ mechanical fatigue limit $>$ electrical fatigue limit. Fracture surface morphologies were observed using scanning electron microscopy-energy dispersive x-ray spectroscopy and electron probe micro-analysis to clarify the fatigue fracture mechanism and to examine the influence of the architecture of the CC tapes on fatigue behaviors. Damage along the edges, caused by slitting during fabrication of the 4 mm wide CC tapes, generated a stress concentration, eventually resulting in earlier crack initiation not only on the substrate, reducing mechanical fatigue strength, but also on the superconducting layer, degrading the measured critical current.

Keywords: coated conductor, fatigue behavior, mechanical and electromechanical properties, electric fatigue limit, CC tape width

(Some figures may appear in colour only in the online journal)

1. Introduction

Because second-generation (2G) high-temperature superconducting (HTS) $(RE)Ba_2Cu_3O_{7x}$ (REBCO) coated conductor (CC) tapes can transport current efficiently and are not particularly vulnerable to high magnetic fields, they are advantageous compared to 1G HTS tapes. Their promising performance has allowed a wide area of practical applications. They are now

being utilized to device applications such as the 45-T superconducting magnet [1], a 10 MW-class superconducting wind power generator [2], superconducting magnetic energy storage units, and nuclear magnetic resonance reactors [3, 4]. Unlike the 1G HTS silver (Ag)-sheathed multifilamentary BSCCO tapes, the REBCO tapes have a superconducting (SC) layer that is deposited on a metallic substrate using a thin film-deposition method, one expansively used with 2G CC tapes [4]. Various deposition methods have been developed and have improved both the performance of REBCO tapes and the process for mass producing them [5–12].

Generally, the critical current, I_c, of CC tapes sensitively depends on the strains and stresses applied during fabrication, cooling, and operation. The mechanism by which I_c degrades can be attributed to various types of damage induced in the SC layer, limiting the efficiency in current transport. An important factor to be considered in device design is the stress and/or strain induced in these tapes during fabrication. For instance, mechanical deformation on CC tapes can be best represented by mechanical response of the SC layer through strain effect on the I_c behavior. It is a well-known fact, according to several literatures [13–15], asserting that when the strain or stress induced to the CC tape exceeded the irreversible strain/stress limit, the I_c will significantly degrade. Additionally, use of the superconducting device subjects the tapes to repeated or cyclic loading such as the thermal stress induced by repeated cool-downs and warm-ups, Lorentz forces induced during coil operation, and alternating centrifugal forces in a motor or generator application. These types of cyclic loadings affect I_c even when the maximum stress level applied was kept below the reversible stress limit for I_c degradation. As a result, the reliability of these CC tapes is threatened.

In many studies, uniaxial tension tests were conducted to evaluate the mechanical and electromechanical properties of 2G CC tapes. Of particular interest were design characteristics regarding on the yield stress (σ_y) and the irreversible stress/strain limits ($\sigma_{irr}/\varepsilon_{irr}$) for I_c degradation at 77 K and self-field or at cryogenic temperatures and low or high magnetic field conditions [16–20].

On the other hand, few studies have focused on evaluating the reliability of CC tapes and their fatigue behaviors. For instance, Ekin *et al* analyzed the transverse fatigue stress tolerance of ion-beam assisted deposition (IBAD)/yttrium barium copper oxide (YBCO) CC tapes used in magnet applications and found that J_c can degrade 2% after 2000 cycles of transverse-direction fatigue at 122 MPa stress amplitude [21]. Sugano *et al* reported high-cycle fatigue behaviors in IBAD/YBCO CC tapes, concluding that fatigue damage in the Ag stabilizing layer is the primary cause of I_c degradation under high-cycle fatigue [22]. On the other hand, Mbaruku *et al* applied strain-based fatigue, up to 10 000 cycles with a stress ratio (R) of 0.2 or 0.5, to investigate the irreversible I_c degradation in IBAD/MOCVD YBCO CC tapes (manufactured by SuperPower, Inc.) and found that crack formations on tape edges initiated I_c degradation [23]. Rogers *et al* investigated fatigue behaviors in YBCO CC tapes from the same manufacturer [24] and GdBa$_2$Cu$_3$O$_y$
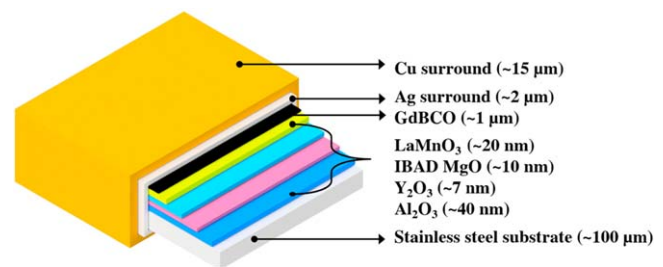

Figure 1. Structure of the supplied ion-beam assisted deposition (IBAD)/reactive co-evaporation by deposition and reaction (RCE-DR)-processed GdBa$_2$Cu$_3$O$_y$ (GdBCO) coated conductor (CC) tape.

(GdBCO) CC tapes manufactured by SuNAM Co., Ltd [25], finding that electrical failure was caused by the slitting process used to reduce conductor width. However, in most cases, those fatigue tests were conducted at room temperature, then I_c measurement at 77 K followed, using a multiple specimen test method. It will show different I_c degradation behaviors when compared to the cases that specimens were fatigue tested at 77 K. In addition, Chen *et al* recently investigated I_c degradation with YBCO CC tapes fatigue applied at 77 K and under a very low magnetic field, finding that electromechanical fatigue properties became less sensitive to the applied magnetic field [26].

Although these studies are relevant evaluations of the fatigue properties of REBCO CC tapes, data that comprehensively characterizes the mechanical and electromechanical fatigue properties of Cu-stabilized REBCO CC tapes (4 and 12 mm widths) at 77 K and their correlations with uniaxial tension stress are currently limited or unavailable. Furthermore, the fatigue mechanisms in multi-layered tapes have not been fully analyzed employing fractographic observations of tape cross-sections and surface morphologies.

The authors' group recently evaluated the electrical and mechanical fatigue limits of various superconductors (e.g. Bi-2223 [27], IBAD/EDDC-SmBCO [28], and IBAD/RCE-DR GdBCO [29]) under high-cyclic loading as found in the practical operating environment. In practical applications where fatigue loading conditions are certain, the mechanical and electrical fatigue strengths or limits are of great importance in the design of superconducting devices. However, studies of high-cycle uniaxial fatigue tests on 2G CC tapes at temperatures of 77 K or lower remain limited, and the definition of the electrical fatigue limit ($\sigma_{fl,elec}$) corresponding to the irreversible I_c degradation has not yet been established. High-cycle uniaxial fatigue tests are difficult and time-intensive, but these challenges must be faced to determine the electrical and mechanical fatigue limits at cryogenic temperatures. Nevertheless, the electrical and mechanical fatigue strengths and limits should be determined at conditions that represent practical applications. For example, 4 mm wide CC tapes usually show fatigue cracks initiating at slit edges regardless of the CC tape process, [29]; therefore, comparative tests with 12 mm wide tapes without slit edges should be conducted to clarify the fatigue fracture mechanisms of multi-layered REBCO CC tapes under cyclic loading.
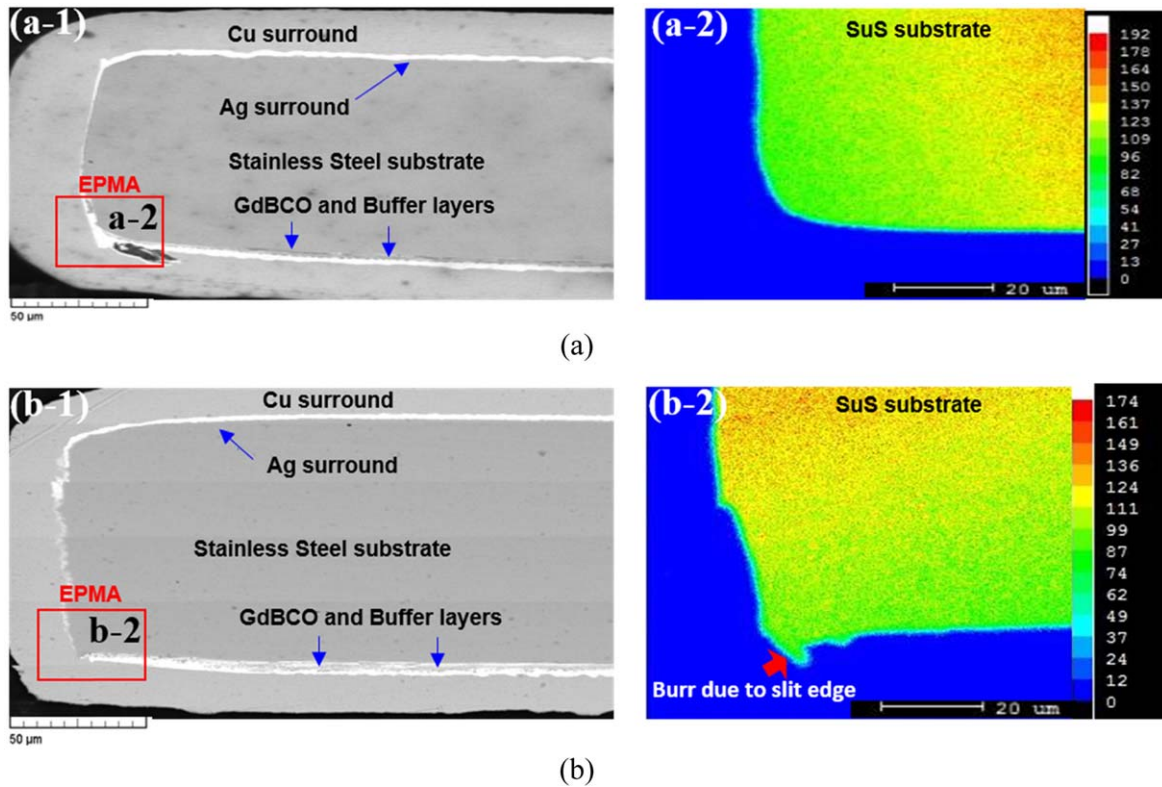
Figure 2. Cross-sectional views of (a) an as-received 12 mm wide GdBCO CC tape and (b) the 4 mm wide CC tape formed by slitting. (a-1) and (b-1) were obtained by scanning electron microscopy; (a-2) and (b-2) by electron probe micro-analysis.

In this study, the mechanical and electromechanical characteristics of GdBCO CC tapes were evaluated under high-cycle uniaxial fatigue conditions at 77 K using two widths of tapes to investigate their fatigue fracture mechanisms. To characterize their electromechanical fatigue behaviors and fatigue fracture mechanisms, micrographs of the as-received specimens were observed simultaneously with the fractography of specimens fatigued at 77 K using optical microscopy, scanning electron microscopy-energy dispersive x-ray spectroscopy (SEM-EDS), and electron probe micro-analysis (EPMA). The influence of the architecture of these tapes on their mechanical and electromechanical fatigue strengths was explained by the initiation and growth behaviors of cracks or defect-like damages observed upon repeated cycling.

2. Experimental procedure

2.1. CC tape samples

The structures and specifications of the IBAD/GdBCO CC tapes fabricated by the reactive co-evaporation by deposition and reaction (RCE-DR) process [30] are shown in figure 1 and table 1. A LaMnO$_3$-buffered IBAD-MgO on a $\sim$100 μm thick stainless-steel substrate was used as a template for the GdBCO layer. The 12 mm wide tape was wrapped in $\sim$2 μm Ag by sputtering. Here, the 12 mm wide tape was compared to a 4 mm wide tape produced by slitting the former using a double-shearing process and rotary slitters. Each was

encapsulated in 15 μm Cu stabilizer using an electroplating process. The supplied samples were not of the same batch and exhibited different I_c values. A recently supplied sample of the 12 mm width had a comparatively large I_c.
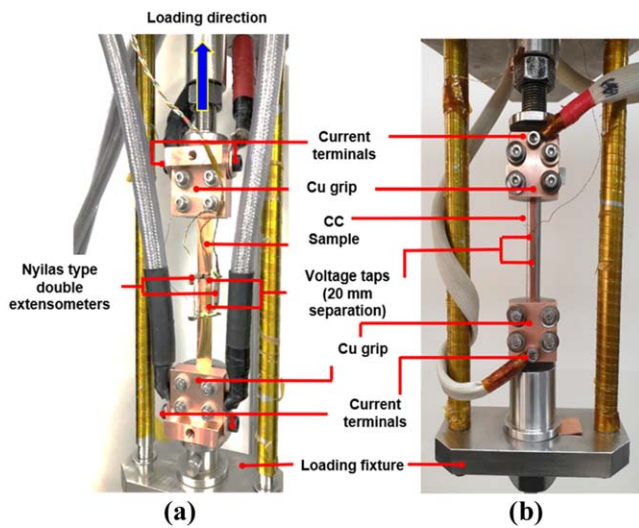
To examine the effect of slitting on the mechanical and electromechanical properties, the edges of both widths of tapes were observed. Figure 2 shows cross-sectional views of the GdBCO CC tapes used in the fatigue test, applying both SEM-EDS ((a-1) and (b-1)) and EPMA ((a-2) and (b-2)). Slitting process implants in the edges are visible on the 4 mm wide tape. The deformed edges in the stainless-steel substrate, clearly shown on the 4 mm wide sample, resemble a burr-like structure (figure 2(b-2)).

2.2. Test procedures at 77 K

Prior to the fatigue test, monotonic uniaxial tension tests using the set-up shown in figure 3(a) were conducted at 77 K to determine σ_y and σ_{irr} for I_c degradation in RCE-DR-processed GdBCO CC tapes. These values will be used as references when determining the maximum stress level that will be adopted in the high-cycle fatigue tests [26, 28]. The experimental set-up for the high-cycle uniaxial fatigue test is shown in figure 3(b). In both tests, the overall length of the CC tapes was 120 mm, and the gage length between the gripping holders was 60 mm. Glass fiber reinforced polymer sheets were inserted between each gripping block and the tape to provide electrical insulation, and emery papers were also inserted to prevent the tape from slipping out of the holder during testing.

Table 1. Specifications of the IBAD/RCE-DR-processed GdBCO CC tape.

Specification of CC samples		
Fabrication process	RCE-DR	
Structure	Ag/GdBCO/LaMnO$_3$/	
	Homo-epi MgO/IBAD MgO/	
	Y$_2$O$_3$/AlO$_3$/Stainless steel/Cu stabilized	
GdBCO film, t	$\sim$1 μm	
Substrate, t	Stainless steel, $\sim$100 μm	
Stabilizer, t	Cu surround, $\sim$15 μm	
Dimension, $t \times w$	0.134 mm $\times$ 12.05 mm	0.130 mm $\times$ 4.05 mm
Critical current (I_c)	$\sim$850 A	$\sim$230 A
Manufacturer	SuNAM Co.	

Figure 3. Testing the coated conductor (CC) tapes. (a) Set-up for the monotonic uniaxial tension test. (b) Set-up for the high-cycle uniaxial fatigue test including I_c measurement at 77 K.

The monotonic uniaxial tension tests were performed first using a universal testing machine (IS-5G with a load cell capacity of 5 kN; Shimadzu) at a ramp rate of 1 mm min^{-1}. Nyilas-type double extensometers with a gage length of 25 mm was used to measure the tensile strain induced in the CC tape sample. To measure I_c, two voltage taps were soldered to the tape near the center of the gage length, 20 mm apart. The four-probe method was used to obtain the voltage (V)–current (I) curve at 77 K and self-field. The curve was used to determine I_c using an electric field criterion of 1 μV cm^{-1} and the transition index (n-value) was obtained in the voltage range of 0.5–2.5 μV cm^{-1}. The reversibility of I_c degradation was checked using a loading–unloading scheme: load was applied at 0.05% strain increments, unloading each time to 10 N followed when $\sim$5% I_{c0} degradation occurred during testing [29, 31]. The irreversible stress/strain limit, $\sigma_{irr}/\varepsilon_{irr}$, corresponding to crack initiation on the GdBCO superconducting film was determined using the 99% I_{c0} recovery criterion [31]. In addition, the 95% I_{c0} retention criterion during loading was determined for comparative purposes.

In the fatigue test, a CC tape was subjected to cyclic tension-tension stress using a hydraulic servo-testing machine (type 8516 with a 5 kN load capacity; Instron). The stress ratio, defined as the ratio between the minimum and maximum stresses applied ($R = \sigma_{min}/\sigma_{max}$), was set to $R = 0.1$. Maximum stress was determined based on σ_y, obtained from the monotonic uniaxial tension test. Here, at the maximum stress level applied, a single sample was used to fatigue test subjecting to repeated cycles continuously with simultaneous I_c measurement at specified repeated cycles. The I_c and n-value at the unstrained initial state were measured before the first fatigue cycle and referred to as I_{c0} and n_0, respectively. During the high-cycle uniaxial fatigue test, I_c was measured at the applied mean stress ($\sigma_{mean} = (\sigma_{max} + \sigma_{min})/2$), at respective specified numbers of cycles (i.e. 10, 50, 100, 5×10^2, 1×10^3 cycles, etc) using a single specimen. Fatigue loading frequencies of 1 and 10 Hz were used: 1 Hz at below 10^3 cycles and 10 Hz at 10^3 cycles or more. Afterward, I_c was continuously measured until 1×10^6 cycles was reached or until current could no longer be transported (i.e. when I_c has significantly degraded even though the CC tape did not fail), or until the CC tape failed. To prevent the failure due to soldering the voltage taps, low-melting-point solder, In$_{52}$Sn$_{48}$ ($T_m = 118$ °C), was used.

The microstructures of the as-received CC tapes and the fractography of the fatigued tapes were observed using optical microscopy (SZ60; Olympus) and SEM-EDS (VEGA II LMU; Tescan). The as-received GdBCO CC tapes were cleansed using a two-step etching process wherein the Cu layer was removed using 30/70 v/v HNO$_3$ in H$_2$O and, after rinsing in water and air-drying, the Ag layer was removed using 25/25/50 v/v/v H$_2$O$_2$, NH$_4$OH, and H$_2$O. After again rinsing in water and air-drying, microstructure observations were made.

3. Experimental results

3.1. Evaluation of characteristic properties in GdBCO CC tapes using uniaxial tension tests at 77 K

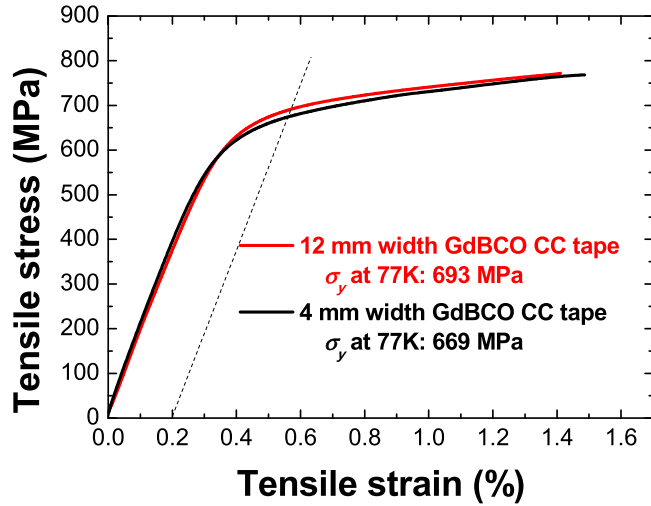Figure 4 shows the tensile stress–strain curves obtained from the uniaxial tension tests at 77 K. It demonstrates that σ_y,

Figure 4. Stress–strain curves obtained from the uniaxial tensile tests at 77 K.

Figure 5. Normalized critical current, I_c/I_{c0}, as a function of tensile stress obtained from electromechanical tests at 77 K.

based on a 0.2% offset strain, was not distinctly different between the 4 mm wide and 12 mm wide CC tapes, which exhibited a mean value of 669 MPa and 693 MPa, respectively. Young's moduli, initially identical, began to diverge at approximately 588 MPa, resulting in a greater yield stress in the 12 mm wide tape by 24 MPa. The stress–strain curves can be used to predict that damage onset, which might have caused the I_c degradation and presumably corresponds to the start of plastic deformation, is closely related to σ_y in both tape widths. The results were validated by carrying out electromechanical tests and determining σ_{irr} for the I_c degradation induced during the loading portion of the loading–unloading scheme. As shown in figure 5, when applying the 99% I_{c0} recovery criterion, σ_{irr} was 660 MPa and 689 MPa for the 4 mm and 12 mm wide tapes, respectively. Because σ_{irr} conformed well to the mechanical yield strength, the σ_{max} adopted for the fatigue test was determined based on the σ_y obtained using the uniaxial tension test at 77 K.

3.2. Evaluation of the mechanical fatigue properties of CC tapes (*S–N curves*) at 77 K

To examine the fatigue characteristics of GdBCO CC tapes at 77 K, high-cycle uniaxial fatigue tests were carried out at $R = 0.1$. Figure 6 shows the *S–N* curves representing the relationship between σ_{max} and the number of cycles to failure (N_f). A near-linear relationship between the maximum stress corresponding to the fatigue strength of CC tape and log N_f is seen for both tape widths. The curve for the 4 mm wide tapes is about 70 MPa lower at any given N_f compared to the 12 mm wide tapes, indicating a lower fatigue strength. Because both widths of tape are composed of essentially the same layers and have the same structure, they are expected to have the same fatigue strength. The only differing factor is the slit edges on the 4 mm wide tapes; therefore, these edges are suspected of influencing the fatigue strength, allowing earlier crack initiation. Fatigued fracture surface morphologies were observed to understand the differences. On the other hand, in light of the conditions under which the CC tape is applied,
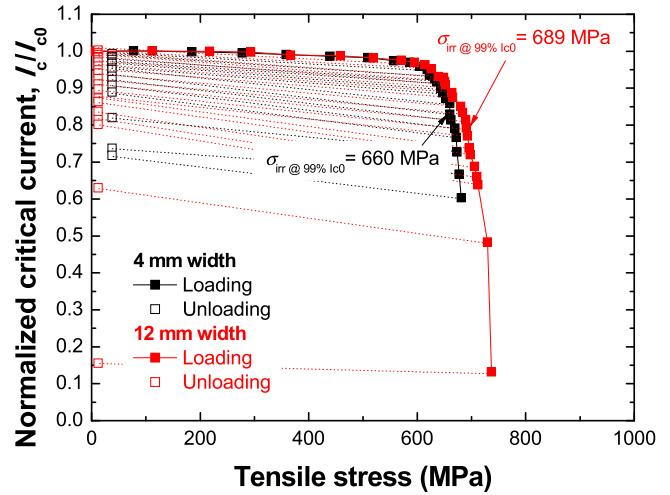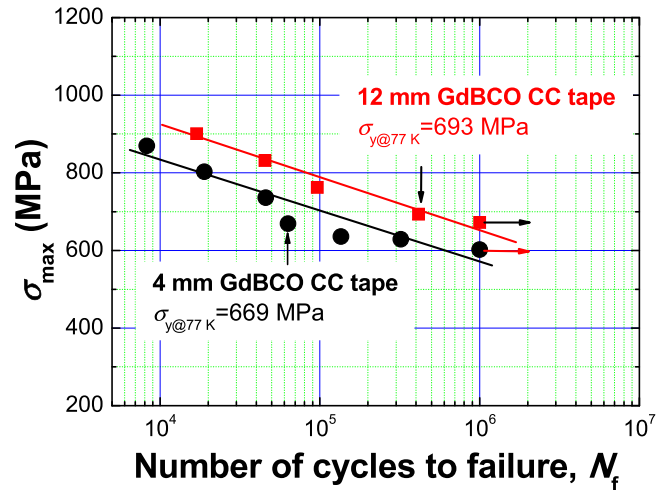

Figure 6. *S–N* curves obtained from fatigue tests at 77 K on RCE-DR processed 4 mm and 12 mm wide GdBCO CC tapes. The sideways pointing arrows → indicate that samples did not fail mechanically and reached the mechanical fatigue limit at 1×10^6 cycles.

such as cyclic loading caused by Lorentz forces or alternating centrifugal forces, the mechanical fatigue limit, $\sigma_{fl,mech}$, could be defined as the fatigue strength at 1×10^6 cycles [27, 28]. This limit is 609 MPa for the 4 mm wide tape and 679 MPa for 12 mm wide tape. When these CC tapes were tested at the σ_{max} lower than the $\sigma_{fl,mech}$, they did not fail at 1×10^6 cycles and were deemed to have infinite lives.

3.3. Evaluation of I_c degradation behaviors in GdBCO CC tapes using high-cycle uniaxial fatigue tests

During the fatigue tests, I_c was measured at specified repeated number of cycles and then normalized by dividing by I_{c0}. Figures 7(a) and (b) shows the variation of the normalized I_c (I_c/I_{c0}) at increasing number of cycles and respective σ_{max} levels for 4 mm wide and 12 mm wide tapes, respectively. Fatigue tests continued until either mechanical failure occurred or current was not longer transported.
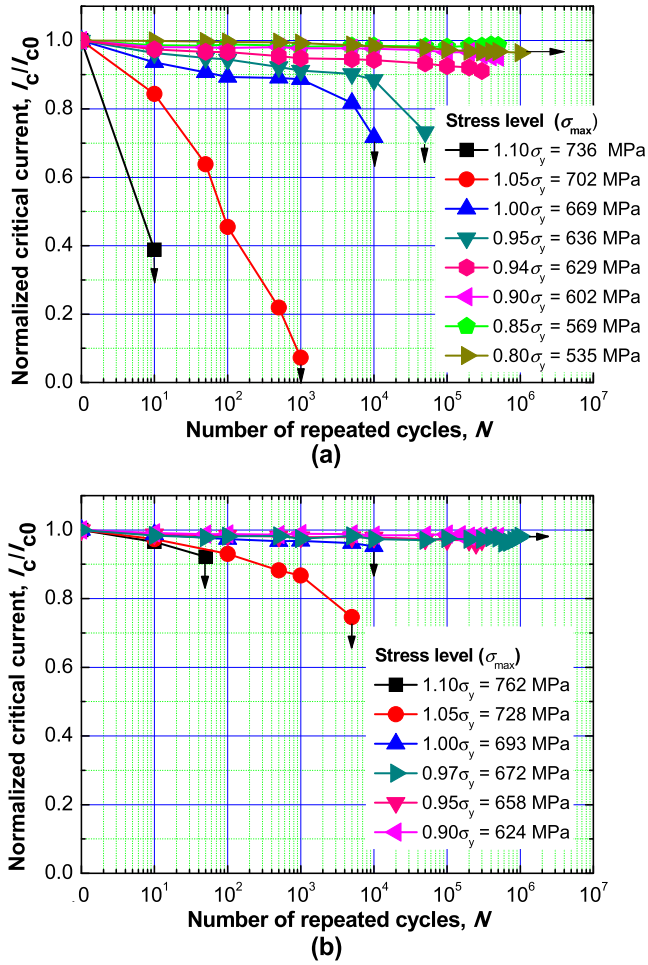
(a)

(b)

Figure 7. Relationship between I_c/I_{c0} and N, determined from fatigue tests on (a) 4 mm wide and (b) 12 mm wide GdBCO CC tapes. When mechanical failure occurred before measuring I_c at the next specified number of cycles, this is indicated by $\downarrow$. The sideways pointing arrows $\rightarrow$ indicate that samples did not fail mechanically and reached the mechanical fatigue limit at 1×10^6 cycles.

Figure 7(a) shows that I_c did not degrade in the 4 mm wide CC tapes when $\sigma_{max} \leqslant 0.90 \ \sigma_y$ (602 MPa) up to 1×10^6 cycles. However, it did degrade gradually, and this degradation became irreversible after 1×10^3 cycles when $\sigma_{max} = 0.94 \ \sigma_y$ (629 MPa). On the other hand, when $\sigma_{max} = 0.95 \ \sigma_y$ (636 MPa), fatigue life was 5×10^4 cycles, where the arrow $\downarrow$ indicates the case that mechanical failure occurred before measuring I_c at the next specified repeated cycles. Upon increasing σ_{max} to 1.0 σ_y (669 MPa), I_c degradation exceeded 5% I_{c0}, even at 10 cycles, showing that the number of cycles at which I_c starts to degrade irreversibly varied depending on σ_{max}. Because I_c degradation was not observed at $\sigma_{max} \leqslant 0.90 \ \sigma_y$ (602 MPa), the critical number of cycles inducing irreversible I_c degradation is expected to vary between $\sigma_{max} = 0.91\sigma_y$ and $\sigma_{max} = 0.93\sigma_y$. Nevertheless, I_c degraded gradually, suggesting that the cracks in the tapes propagated slowly throughout repeated cycling, eventually accelerating I_c degradation. Comparatively, I_c degradation was sharp and fatigue life was shorter when $\sigma_{max} \geqslant 1.05 \ \sigma_y$, as shown in figure 7(a). Electrical and mechanical fatigue limits were reached in some samples even though the applied

stress did not incur significant I_c degradation. These samples did not electrically or mechanically fail even at 1×10^6 cycles. The electrical fatigue limit, $\sigma_{fl,elec}$, was obtained from the I_c degradation behaviors at 1×10^6 cycles using the 95% I_c retention criterion for each σ_{max}. This limit is corresponding to 0.90 σ_y (602 MPa) for the 4 mm wide CC tape.

Figure 7(b) shows the I_c degradation behaviors for 12 mm wide CC tapes at increasing numbers of cycles and specified σ_{max} levels, revealing that compared to 4 mm wide tapes, I_c degraded less even when σ_{max} was close to $1.0\sigma_y$. Of the two, the 12 mm wide tapes were superior in electrical fatigue strength. Even at $0.97\sigma_y$ (672 MPa), I_c did not degrade, and the mechanical fatigue limit of 1×10^6 cycles was reached. In fact, I_c only begins to degrade, and in a gradual manner, when $\sigma_{max} = 1.0\sigma_y$, but the tape ceased transporting current at 1×10^4 cycles due to mechanical failure before I_c could be measured at the next specified number of cycles. At that stress level, fatigue cracks on the substrate initiated and propagated into the SC layer, resulting in electrical failure. Upon further increasing σ_{max}, severe I_c degradation was observed as earlier fatigue failure, and the electrical properties significantly decreased until sample failure. Damage might have occurred in the SC layer in a diverse manner. To clarify the fatigue fracture mechanism, SEM fractographs of fatigued CC tapes were observed in the following section.

To further investigate the fatigue behaviors of I_c, the n-value was derived from the V–I curve using a power law fit ($V = cI^n$). This n-value reflects the abruptness in the transition from the superconducting state to the normal state [32], and it indicates indirectly the extent of damage induced in the SC layer in CC tapes during fatigue loading [33]. Typically, n-values range from 10 to 100 and highly depend on the homogeneity in the CC tape, particularly in the SC layer. A low n-value accompanied by scattered values/transitions is associated with nonuniformity in the CC tape created by cracking, etc [32]. Figure 8 shows, for each tape width, the relationship between the normalized n-value, calculated by dividing it by n_0, and the number of repeated cycles. The two tape widths show similar variations, supporting the I_c/I_{c0}–N behaviors observed in figure 7. The 4 mm wide tapes showed no significant variation in n-value when $\sigma_{max} \leqslant 0.94 \ \sigma_y$; cracks did not form, I_c degradation was not seen, since the fatigue test condition was below the mechanical fatigue limit of the tape.

Figure 8(b) shows the n/n_0–N relationships for the 12 mm wide GdBCO CC tapes, demonstrating similarities with the I_c/I_{c0}–N relationships shown in figure 7(b), thereby confirming an indirect relationship between the n-value and possible damage to the SC layer, particularly when $\sigma_{max} \geqslant 0.95 \ \sigma_y$. Furthermore, broad scattering is seen in the n-values over the specified numbers of fatigue cycles, more so in the 12 mm wide CC tapes compared to the 4 mm wide tapes. These variations can be linked to the microstructure in the SC layer, where structural discontinuities found along the width or length of the tape can cause changes in fatigue life and in electrical and mechanical fatigue behaviors. This correlation has been suggested by other researchers using similar
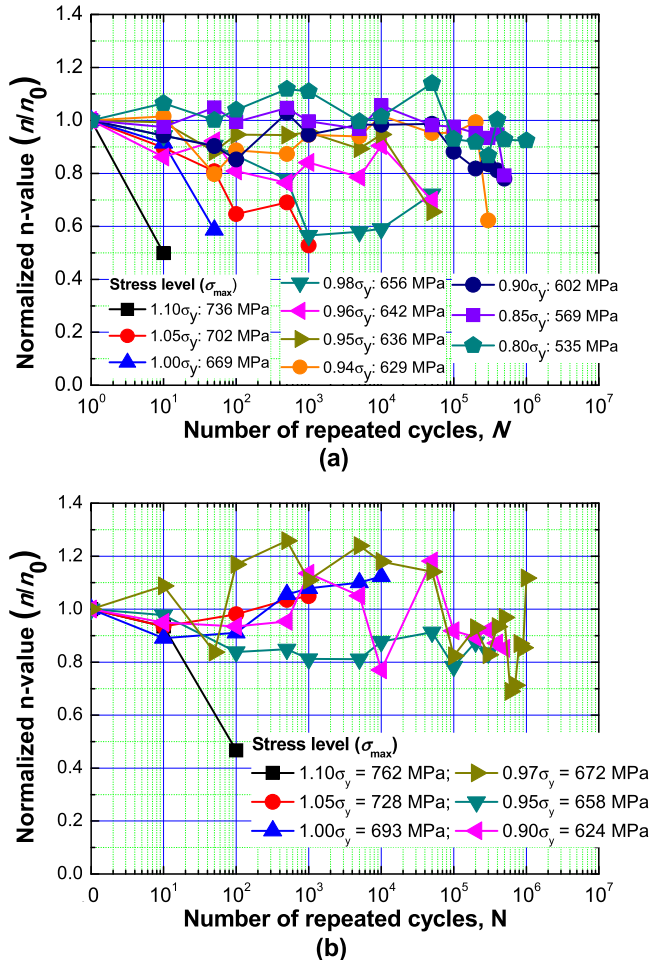
Figure 8. Relationship between n/n_0 and N, determined from high-cycle uniaxial fatigue tests on (a) 4 mm wide and (b) 12 mm wide GdBCO CC tapes.

and different superconducting materials [24, 25, 34]. As a whole, regardless of tape width, the *n*-value dropped sharply when stress was greater ($\sigma_{max} \geqslant 1.0 \ \sigma_y$).

4. Discussion

4.1. Fractographic observations of fatigued GdBCO CC tapes

Figures 9(a) and (b) shows the images, obtained using SEM, of the GdBCO films from the as-received 4 and 12 mm wide CC tapes after etching away the Cu and Ag layers. The 4 mm wide samples were subjected to the slitting process. Aside from that, the tapes were identically handled: no strain or any processing other than etching was applied to either tape. Figure 9(a) shows that, on the 4 mm wide tape, microcracks formed at the slit edge and propagated inward at an inclined angle of ~45°, averaging 60 μm in length, and that approximately 20 μm from the edge, portions of the SC layer were removed due to damage. It also shows that the burr created at the tape edge during slitting pushed the SC layer, causing it to deform or delaminate, consequently removing a part of the SC layer at the edges and creating surface

microcracks (defects) near the edge. Comparatively, the 12 mm wide tape (figure 9(b)) shows no visible microcracks or damage to the SC layer along the edge.

To examine how the microcracks observed in the as-received 4 mm wide CC tapes evolved during the fatigue test, images after fatigue tests at various σ_{max} levels were obtained and shown on figure 10. At $\sigma_{max} = 0.85 \ \sigma_y$ (569 MPa), the surface morphology is nearly identical to that observed in the as-received CC tape (figure 9(a)): microcracks were distributed randomly along the edge with an inclined orientation, and portions of the SC layer along the edge were removed. At this σ_{max}, I_c did not degrade up to the fatigue limit of 1×10^6 cycles. At $\sigma_{max} = 0.90\sigma_y$ (602 MPa), microcracks were slightly more developed but limited to the edge of the tape (figure 10(b)). Again, no I_c degradation was observed up to 1×10^6 cycles. Finally, at $\sigma_{max} = 0.95\sigma_y$ (636 MPa), the damage induced in the SC layer by the microcracks was severe and extended to the ceramic buffer layers of the tape (figure 10(c)). A delaminated or detached SC layer was observed, covering nearly 80 μm of the edge toward the center of the tape. Instead, the localized regions where the SC layers are randomly present, like at $\sigma_{max} = 0.90\sigma_y$, are no longer observed. This observation is considered valid, knowing that the failure mode in these CC tapes is caused primarily by interfacial debonding of the layers (delamination). Furthermore, the electrical fatigue strength was quite low at this σ_{max}, I_c degraded momentarily after only 50 cycles, and the CC tape mechanically failed at ~1.35×10^5 cycles.

Surface micrographs, obtained using SEM, of the fatigue-tested 12 mm wide CC tapes are shown in figures 11 and 12. At $\sigma_{max} = 0.95\sigma_y$ (658 MPa), no cracks are visible on the surface of the tape. However, upon careful examination under higher magnification, nano-sized cracks are found, scattered transversely to the loading direction. These nano-sized cracks are not considered to represent the initiation of cracks, as are the microcracks visible at the surface edges of the 4 mm wide tape. Additionally, no I_c degradation occurred up to 1×10^6 cycles, confirming that the nano-sized cracks did not represent the initiation of fatigue cracks that can ultimately influence the electrical and mechanical fatigue behaviors of the CC tapes.

When $\sigma_{max} = 1.0\sigma_y$ (693 MPa), I_c degraded significantly, revealing that multiple cracks had formed on the SC layer of the 12 mm wide fatigue-tested tape perpendicular to the loading axis (figure 11(b)). Differing from observations seen at lower values of σ_{max}, significant microcracks were noticeable and originated at the tape edge, where localized delamination of the SC layer was evident. Cracks were also observed near the center of the tape, indicating that the cracks initiating at the edges propagated to the center as cycling progressed. The crack density in the center of the tape was lower than that along the edges. These cracks might be able to induce other forms of damage such as delamination of the SC layer, which can subsequently lead to electrical failure and apparent mechanical failure as cycling continues.

Figure 12 shows the surface morphology of a 12 mm wide CC tape that failed both electrically and mechanically
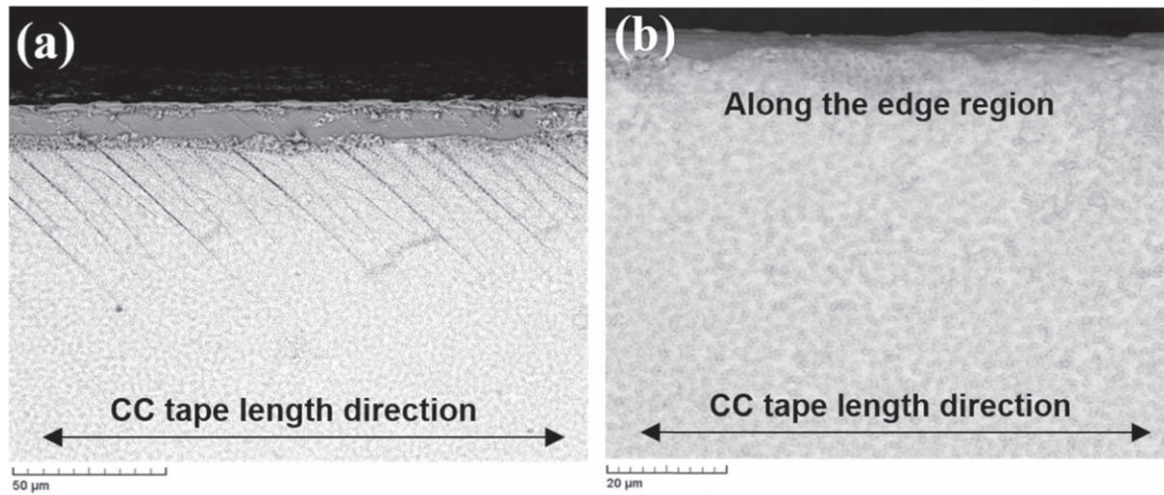
Figure 9. Surface microstructures of the GdBCO superconducting layer in as-received (a) 4 mm and (b) 12 mm wide CC tapes, observed using SEM after etching.
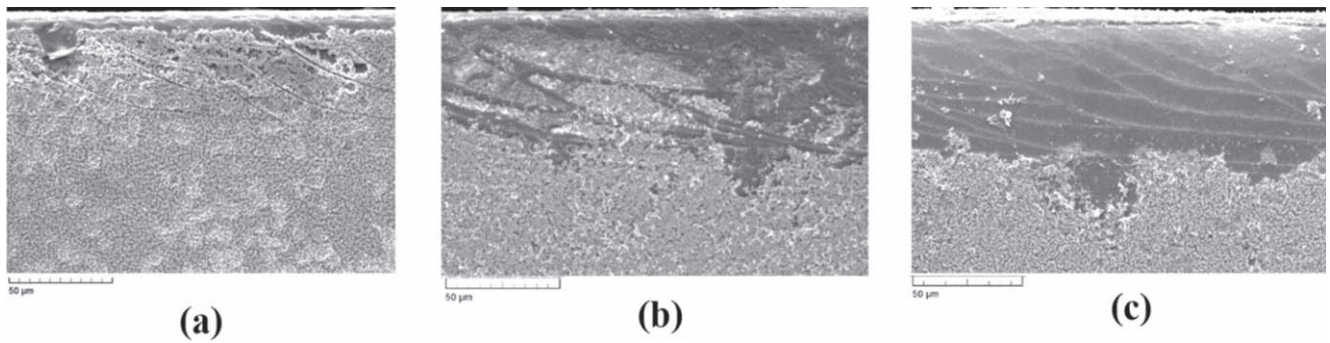

Figure 10. SEM micrographs at the surfaces of fatigue-tested 4 mm wide GdBCO CC tapes, observed after etching. Applied maximum stress in the fatigue tests were (a) 0.85 σ_y (569 MPa), (b) 0.90 σ_y (602 MPa), and (c) 0.95 σ_y (636 MPa).
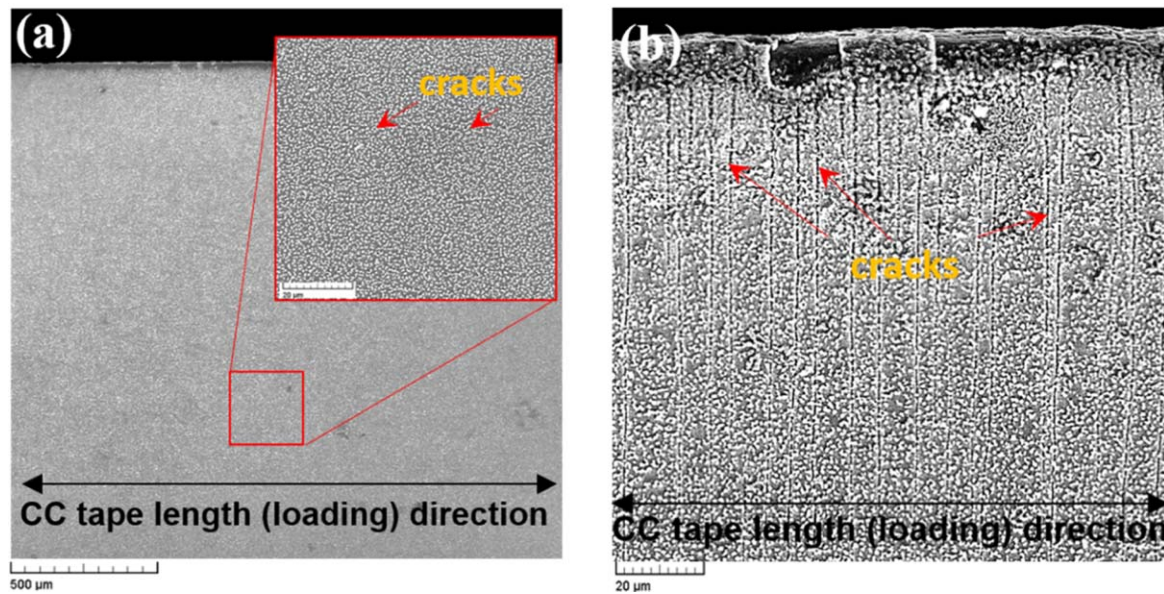

Figure 11. SEM micrographs of the surfaces of fatigue-tested 12 mm wide GdBCO CC tapes after etching. (a) $\sigma_{max} = 0.95\ \sigma_y$ (658 MPa); (b) $\sigma_{max} = 1.0\ \sigma_y$ (693 MPa).
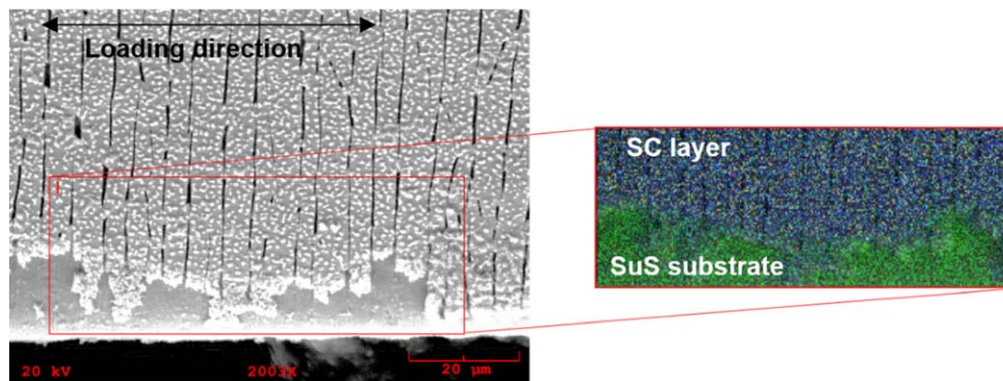
Figure 12. Surface morphology of a 12 mm wide GdBCO CC tape fatigue-tested at $\sigma_{max} = \sim800$ MPa, etched, then observed using SEM-EDX. The overlay showing the elements at the edge suggests that delamination occurred during the fatigue test.

after a relatively small number of cycles at $\sigma_{max} = \sim800$ MPa. Significant transverse cracks formed evenly on the entire surface of the tape. Delamination of the GdBCO layer is also evident along the edge, as shown by the EDS segment, identifying the elements of the image. The parallel orientation of the cracks suggest that they proceeded from the edge toward the center of the tape. The uniformity in the crack pattern suggests that they might not have originated from the grain boundaries in the GdBCO layer. Instead, it is most likely that the fatigue crack initiation was influenced by coalescence of microcracks in the stainless-steel substrate as well as substrate yielding.

4.2. Comparisons of characteristic fatigue properties of GdBCO CC tapes at 77 K

In this study, uniaxial tension tests and high-cycle uniaxial fatigue tests were performed at 77 K to obtain reliability-related characteristics of GdBCO CC tapes. Additionally, test procedures to obtain the characteristic properties of CC tapes could be established. Certain correlations were found between the mechanical and electromechanical properties obtained using both tests.

Figure 13 shows the mechanical and electrical fatigue strength behaviors for the two widths of CC tapes across a specified range of fatigue cycles. The electrical fatigue strength behavior was obtained from the stress value defined using the 95% I_{c0} retention criterion over the range of cycles. Because both widths of CC tapes were subjected to the same fatigue conditions, their electromechanical fatigue behaviors were expected to be similar. However, the 4 mm wide CC tapes produced fatigue limits that were a bit lower than those produced by the 12 mm wide tapes, both electrically and mechanically. For instance, at σ_y (669 MPa for the 4 mm wide tape and 693 MPa for the 12 mm wide tape), significant differences were found in the number of cycles to electrical failure (where I_c degradation occurred below the 95% I_c retention) and mechanical failure (the stress at which failure occurs). Also, compared to the mechanical fatigue strengths, the electrical fatigue strengths were such that failure occurred after quite a lower number of cycles. As σ_{max} decreases for
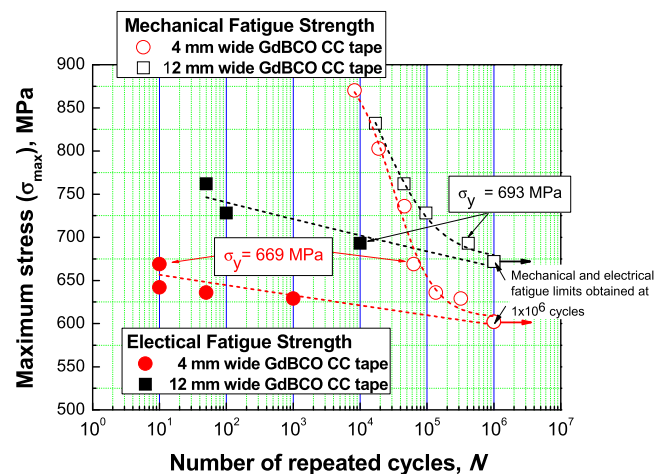

Figure 13. Mechanical and electrical fatigue strength behaviors with increasing number of fatigue cycles for 4 and 12 mm wide GdBCO CC tapes at 77 K.

each tape width, the number of cycles it takes to incur electrical failure noticeably increases.

Table 2 shows all the characteristic properties determined for the two tape widths from the uniaxial tensile and high-cycle uniaxial fatigue tests at 77 K. For both widths, the characteristic strengths follow a pattern: $\sigma_y > \sigma_{irr} > \sigma_{fl.mech} > \sigma_{fl,elec}$, where the lowest strength is demonstrated at the electrical fatigue limit ($\sigma_{fl,elec}$). In general, the 4 mm wide tapes exhibited lower strength limits than the 12 mm wide tapes. The difference became larger in the cases obtained from high-cycle fatigue tests, which indicates that the damage at slit edge was more affected the reliability related property of fatigue strength.

Thus, it is apparent that the electrical fatigue strength of a CC tape relied on the fracture characteristics of the SC layer, but the substrate largely influenced the mechanical fatigue strength. Because the SC layer is considered to be brittle, the overall performance of a CC tape will be highly dependent on the layer that will fracture or yield first. This suggests that the surface structure of a CC tape must be carefully processed during manufacturing of its constituent layers so that cracking is suppressed, especially at the edges of the CC tapes.

Table 2. Mechanical and electromechanical properties obtained from monotonic tensile tests and high-cycle uniaxial fatigue tests at 77 K.

RCE-DR GdBCO	Uniaxial tensile test		High cycle uniaxial fatigue test	
	Yield stress (σ_y), MPa (0.2% *offset strain*)	Irreversible stress limit (σ_{irr}), MPa (99% I_{e0} *recovery criterion*)	Mechanical fatigue limit ($\sigma_{fl\ mech}$), MPa (*at* 1×10^6 *cycles*)	Electrical fatigue limit ($\sigma_{fl\ elec}$), MPa (*at* 1×10^6 *cycles*)
4 mm wide	669	660	609	602
12 mm wide	693	689	679	672

5. Conclusions

Through high-cycle uniaxial fatigue tests, the electrical and mechanical fatigue performances of 4 mm wide and 12 mm wide GdBCO CC tapes were investigated at $R = 0.1$ and 77 K. The width of the CC tape was found to influence its strength characteristic properties. Damage caused to a CC tape by slitting caused stress concentration at the edges of the tape, becoming enough to cause crack initiation in the SC layer, resulting in earlier I_c degradation. The 4 mm wide tape showed fatigue limits that were a lower than those shown by the 12 mm wide tape, both in electrical and mechanical aspects. The 12 mm wide tape showed superior fatigue strength compared to the 4 mm wide tape, especially in mechanical aspects. Microcracks observed at the edges of the as-received 4 mm wide CC tape propagated across the width of the tape as the applied stress increased during fatigue loading, causing damage such as cracking and delamination in the SC and buffer layers. The relationships between N and both normalized I_c and n-value behaved similarly for the two tape widths, resulting in a sequence in the obtained characteristic strengths that was the same for both: $\sigma_y > \sigma_{irr} > \sigma_{fl,mech} > \sigma_{fl,elec}$. The electrical fatigue limit ($\sigma_{fl,elec}$) exhibited the lowest strength. Through fractographic observations, the electrical fatigue strength of a CC tape was found to depend primarily on the fracture behavior in the SC layer; the mechanical fatigue strength, on the other hand, was predominantly influenced by the substrate.

Acknowledgments

ORCID iDs

Hyung-Seop Shin ⬤ https://orcid.org/0000-0002-4922-2427

References

[1] Hahn S *et al* 2019 45.5 Tesla direct-current magnetic field generated with a high-temperature superconducting magnet *Nature* **570** 496–9
[2] Snitchler G, Gamble B, King C and Winn P 2011 10 MW class superconductor wind turbine generators *IEEE Trans. Appl. Supercond.* **21** 1089–92
[3] Ohshima S, Hoshi H, Takanashi N, Yamada H, Saito A, Yoshioka E, Sekiya N, Tsuji S and Suematsu H 2019 Examination on high-Q NMR transmit/receiver pick-up coils made by YBaCuO thin films *IEEE Trans. Appl. Supercond.* **29** 5
[4] Mukherjee P and Rao V 2019 Design and development of high temperature superconducting magnetic energy storage for power applications—a review *Physica* C **563** 67–73
[5] Norton D *et al* 1996 Epitaxial YBa$_2$Cu$_3$O$_7$ on biaxially textured nickel (001): an approach to superconducting tapes with high critical current density *Science* **274** 755–7
[6] Kutami H, Hayashida T, Hanyu S, Tashita C, Igarashi M, Fuji H, Hanada Y, Kakimoto K, Iijima Y and Saitoh T 2009 Progress in research and development on long length coated conductors in Fujikura *Physica* C **469** 1290–3
[7] Rupich M W *et al* 2010 Advances in second generation high temperature superconducting wire manufacturing and R&D at American superconductor corporation *Supercond. Sci. Technol.* **23** 014015
[8] Selvamanickam V *et al* 2009 High performance 2G wires: from R &D to pilot-scale manufacturing *IEEE Trans. Appl. Supercond.* **19** 3225–30
[9] Oh S S *et al* 2008 Development of long-length SmBCO coated conductors using a batch-type reactive co-evaporation method *Supercond. Sci. Technol.* **21** 034003
[10] Matias V, Rowley E J, Coulter Y, Maiorov B, Holesinger T, Yung C, Glyantsev V and Moeckly B 2010 YBCO films grown by reactive co-evaporation on simplified IBAD-MgO coated conductor templates *Supercond. Sci. Technol.* **23** 014018
[11] Matias V and Hammond R H 2012 YBCO superconductor wire based on IBAD-textured templates and RCE of YBCO process economics *Phys. Proc.* **36** 1440–4
[12] Lee J H, Lee H, Lee J W, Choi S M, Yoo S I and Moon S H 2014 RCE-DR, a novel process for coated conductor fabrication with high performance *Supercond. Sci. Technol.* **27** 044018
[13] Osamura K, Machiya S and Hampshire D P 2016 Mechanism for the uniaxial strain dependence of the critical current in practical REBCO tapes *Supercond. Sci. Technol.* **29** 065019
[14] Van der Laan D C, Ekin J W, Douglas J F, Clickner C C, Stauffer T C and Goodrich L F 2010 Effect of strain, magnetic field and field angle on the critical current density of YBa2Cu3O7-δ coated conductors *Supercond. Sci. Technol.* **23** 7
[15] Shin H S, Kim K H, Dizon J R, Kim T Y, Ko R K and Oh S S 2005 The strain effect on critical current in YBCO coated conductors with different stabilizing layers *Supercond. Sci. Technol.* **18** S364
[16] Van der Laan D C and Ekin J W 2007 Large intrinsic effect of axial strain on the critical current of high temperature superconductors for electric power applications *Appl. Phys. Lett.* **90** 052506
[17] Cheggour N, Ekin W, Thieme C, Xie Y, Selvamanickam V and Feenstra R 2005 Reversible axial-strain effect in Y-Ba-Cu-O coated conductors *Supercond. Sci. Technol.* **18** 319–24
[18] Sugano M, Osamura K, Prusseit W, Semerad R, Kuroda T, Itoh K and Kiyoshi T 2005 Irreversible strain dependence of critical current in 100 A class coated conductors *IEEE Trans. Appl. Supercond.* **15** 3581–4
[19] Shin H S, Diaz M A and Lee J H 2017 Characterization of electromechanical properties of Sn-Cu double layer stabilized GdBCO coated conductor tapes at 77 K *Prog. Supercond. Cryog.* **19** 26–30
[20] Bautista Z, Diaz M A, Shin H S and Lee J H 2018 Measurement reliability of irreversible stress / strain limits in Sn-Cu double layer stabilized IBAD / RCE-DR processed GdBCO coated conductor tapes under uniaxial tension at 77 K *Prog. Supercond. Cryog.* **20** 36–40
[21] Ekin J W, Bray S L, Cheggour N, Clickner C C, Foltyn S R, Arendt P N, Polyanskii A A, Larbalestier D C and

McCowan C N 2001 Transverse stress and fatigue effects on Y-Ba-Cu-O coated IBAD tapes *IEEE Trans. Appl. Supercond.* **11** 3389–92

[22] Sugano M *et al* 2008 Two different mechanisms of fatigue damage due to cyclic stress loading at 77 K for MOCVD-YBCO-coated conductors *Supercond. Sci. Technol.* **21** 054006

[23] Mbaruku A L and Schwartz J 2008 Fatigue behavior of Y–Ba–Cu–O/Hastelloy-C coated conductor at 77 K *IEEE Trans. Appl. Supercond.* **18** 1743–52

[24] Rogers S, Chan W K and Schwartz J 2016 Effects of room temperature tensile fatigue on critical current and n-value of IBAD-MOCVD YBa2Cu3O7−x/Hastelloy coated conductor *Supercond. Sci. Technol.* **29** 085013

[25] Rogers S and Schwartz J 2017 Tensile fatigue behavior and crack growth in GdBa$_2$Cu$_3$O$_{7-x}$/stainless-steel coated conductor grown via reactive co-evaporation *Supercond. Sci. Technol.* **30** 045013

[26] Chen W, Zhang H, Chen Y, Liu L, Shi J, Yang X and Zhao Y 2018 Fatigue behavior of critical current degradation for YBCO tapes at 77 K *IEEE Trans. Appl. Supercond.* **28** 8400905

[27] Shin H S, Dizon J R, Kim K H, Oh S S and Ha D W 2005 Mechanical and transport properties of Ag alloy/Bi-2223 superconducting tapes under axial fatigue loading *Physica* C **426-431** 1188–93

[28] Shin H S and Dedicatoria M J 2011 Mechanical and transport properties of IBAD/EDDC-SmBCO coated conductor tapes during fatigue loading *Cryogenics* **51** 237–40

[29] Shin H S *et al* 2016 Evaluation of the electromechanical properties in GdBCO coated conductor tapes under low cyclic loading and bending *Supercond. Sci. Technol.* **29** 014001

[30] Ko K P, Ha H S, Kim H K, Yu K K, Ko R K, Moon S H, Oh S S, Park C and Yoo S I 2007 Fabrication of highly textured IBAD-MgO template by continuous reel-to-reel process and its characterization *Physica* C **463-465** 564–7

[31] Shin H S and Bautista Z 2019 Establishing a test procedure for evaluating the electromechanical properties of practical REBCO coated conductor tapes by the uniaxial tension test at 77 K *Supercond. Sci. Technol.* **32** 064004

[32] Ekin J W 2006 *Experimental Techniques for Low-Temperature Measurement* (Oxford: Oxford University Press)

[33] Goodrich L F, Srivastava A N, Yuyama M and Wada H 1993 n-value and second derivative of the superconductor voltage-current characteristic *IEEE Trans. Appl. Supercond.* **3** 1265–8

[34] Ghosh A K 2004 *V–I* transition and *n*-value of multifilamentary LTS and HTS wires and cables *Physica* C **401** 15–21